World Scientific
www.worldscientific.com

Self-confocal NIR-II fluorescence microscopy for multifunctional *in vivo* imaging

Jing Zhou [ID]*, Tianxiang Wu [ID]*,†, Runze Chen [ID]*, Liang Zhu‡, Hequn Zhang*,‡,
Yifei Li [ID]*, Liying Chen* and Jun Qian*,†,§

*State Key Laboratory of Modern Optical
Instrumentations, Centre for Optical and
Electromagnetic Research, College of Optical
Science and Engineering, International Research
Center for Advanced Photonics, Zhejiang University,
Hangzhou 310058, P. R. China

†Dr. Li Dak Sum & Yip Yio Chin Center
for Stem Cell and Regenerative Medicine, Zhejiang
University, Hangzhou 310058, P. R. China

‡College of Biomedical Engineering and
Instrument Science, Interdisciplinary Institute
of Neuroscience and Technology (ZIINT),
Zhejiang University, Hangzhou 310027,
P. R. China
§qianjun@zju.edu.cn

Fluorescence imaging in the second near-infrared window (NIR-II, 900–1880 nm) with less scattering background in biological tissues has been combined with the confocal microscopic system for achieving deep *in vivo* imaging with high spatial resolution. However, the traditional NIR-II fluorescence confocal microscope with separate excitation focus and detection pinhole makes it possess low confocal efficiency, as well as difficultly to adjust. Two types of upgraded NIR-II fluorescence confocal microscopes, sharing the same pinhole by excitation and emission focus, leading to higher confocal efficiency, are built in this work. One type is fiber-pinhole-based confocal microscope applicable to CW laser excitation. It is constructed for fluorescence intensity imaging with large depth, high stabilization and low cost, which could replace multiphoton fluorescence microscopy in some applications (e.g., cerebrovascular and hepatocellular imaging). The other type is air-pinhole-based confocal microscope applicable to femtosecond (fs) laser excitation. It can be employed not only for NIR-II fluorescence intensity imaging, but also for

§Corresponding author.

multi-channel fluorescence lifetime imaging to recognize different structures with similar fluorescence spectrum. Moreover, it can be facilely combined with multiphoton fluorescence microscopy. A single fs pulsed laser is utilized to achieve up-conversion (visible multiphoton fluorescence) and down-conversion (NIR-II one-photon fluorescence) excitation simultaneously, extending imaging spectral channels, and thus facilitates multi-structure and multi-functional observation.

Keywords: Self-confocal; fiber-pinhole; air-pinhole; multi-channel fluorescence lifetime imaging; multi-color imaging.

1. Introduction

Fluorescence imaging is a widely used optical imaging method with high spatiotemporal resolution and targetable labeling function. It has been widely used in biomedical fields, such as clinical fluorescence navigation surgery, brain science research, angiography, cell/tissue visualization, anti-body labeling, gene expression and gene mapping.[1–12] Two mainstream types of fluorescence microscopy for high-resolution tomography are multiphoton fluorescence microscopy and confocal microscopy. Multiphoton fluorescence microscopy based on the intrinsic nonlinear optical effect has peculiar ability to improve imaging resolution, with high peak power pulsed laser (e.g., femtosecond (fs) laser) excitation. The long-wavelength fs excitation beam can also penetrate deeply and focus well inside biological tissues. With attractive advantages of high spatial resolution and large imaging depth, multiphoton fluorescence microscopy has been extensively utilized in biomedical fields.[13–17] However, one point of concerns is that fs pulsed laser leads to nonnegligible ionizing damage to biological tissues, due to its extremely high peak density.[18] In addition, it has stringent maintenance requirements and high costs.

Fluorescence imaging in the second near-infrared window (NIR-II, 900–1880 nm) for biological tissues has the advantages of larger penetration and high signal-to-background ratio, due to lower optical scattering, larger light absorption, and negligible autofluorescence in biological tissues. Besides, although different wavelength lights have different scattering coefficients (different propagation paths) in the biological tissues, the lower scattering coefficient of longer wavelength light will diminish the impact of scattering and reduce the chromatic dispersion of the tissue. Various imaging modes have been developed, including NIR-II macro-imaging and NIR-II microscopy.[3,5,19–28] As one typical kind of NIR-II microscopic imaging technologies, NIR-II fluorescence confocal microscopy adopts longer-wavelength excitation and emission compared to the existing commercial (visible) confocal microscopy. With longer wavelength, the excitation can penetrate deeper and focus tighter inside biological tissues, and the fluorescence has higher ratio of ballistic and snake photons to diffusive photons (based on the lower optical scattering[20,29] and higher light absorption[22] in the biological tissues), enabling that more fluorescent photons (ballistic and snake) from the focus in the sample can be collected by the detection pinhole, and meanwhile more fluorescent photons (ballistic and snake) from the out-of-focus can be filtered away by the detection pinhole, leading to higher signal to background imaging result with less chromatic dispersion caused by the biological tissues. However, the developed NIR-II fluorescence confocal microscopes still have some annoying points. Due to the low quantum efficiency of NIR-II detector, normally InGaAs photomultiplier tube (PMT), the requirement of conjugation of excitation focus in the sample and the detection pinhole is fairly strict. What adding insult to injury is that the NIR-II fluorescence signal is weak, resulting in the position of detection pinhole to be unpredictable and the alignment to be difficult in the traditional way.

In our work, two types of upgraded NIR-II fluorescence confocal microscope with high detection efficiency and facile adjustment are proposed and constructed. The trick is that conjugating the excitation focus in the sample to the spatial path, and then let the excitation focus on the spatial path coincide with the fluorescence focus, thus it only needs the excitation focus on the spatial path to be located inside the detection pinhole. One type is fiber-pinhole-based and adjustment-free self-confocal NIR-II fluorescence microscope, which is applicable to continuous wave (CW) laser excitation with less ionizing damage to biological tissues. It is mainly utilized for fluorescence intensity imaging, and can selectively replace multiphoton fluorescence

microscopy in some application scenes, such as cerebrovascular imaging, with comparable imaging depth and quality under similar imaging conditions. The other type is air-pinhole-based and easily adjustable self-confocal NIR-II fluorescence microscope, applicable to fs pulsed laser excitation. It can be applied not only in fluorescence intensity imaging, but also in multi-channel fluorescence lifetime imaging to recognize different structures with the similar fluorescence spectrum. What's more, facilely combining multiphoton fluorescence microscopy onto it can achieve up-conversion (visible multiphoton fluorescence) and down-conversion (NIR-II one-photon fluorescence) imaging simultaneously, under the same fs laser excitation. This is a powerful technology for observing multiple biological structures simultaneously and performing multi-functional biological studies.

2. Materials and Methods

2.1. *Materials*

Indocyanine green (ICG) was purchased from DanDong Pharmaceutical Factory (Liaoning, China). DCBT NPs[30] and 2TT-oC26B NPs[31] were synthesized according to our previous reports. CdSe/CdS/ZnS@SH-PEG2000 quantum dots were kindly provided by the prof. Xiaogang Peng group in Zhejiang University. DMSO was obtained from Sinopharm Chemical Reagent Co., Ltd. (Shanghai, China). Deuterium oxide was bought from J&K Scientific (Shanghai, China).

2.2. *Animal and surgery*

C57BL/6 mice (female, 6 weeks old) were used for *in vivo* experiments. They were provided by the Zhejiang Academy of Medical Sciences and kept at the Experimental Animal Center of Zhejiang University. The room temperature of the rearing environment was maintained at 24°C with a 12 h light/dark cycle. Mice were continuously supplied with water and standard laboratory chows. All *in vivo* experiments were strictly abided "The National Regulation of China for Care and Use of Laboratory Animals".

In the cerebrovascular imaging experiments, the skull of the anesthetized mouse was opened by microsurgery. A thin round cover glass was tightly pressed over the brain to protect it as well as hold deuterium oxide (matching liquid of the objective). Then a stainless steel head piece with double wings was attached to the skull of the mouse by glue and reinforced with dental cement. Before imaging, both wings were fixed on the mouse holder to immobilize mouse's head which ensures the stable microscopic imaging. Then the mouse was intravenously injected with ICG for NIR-II fluorescence confocal microscopic imaging or DCBT NPs for multiphoton fluorescence microscopic imaging.

In hepatic imaging experiments, the mouse was anesthetized and shaved, and then the laparotomy was performed to completely expose the liver. Next, a rectangular glass slide with medical adhesive tape to cover its sharp edges and increase its surface friction was placed above the abdominal cavity. Then the large liver lobe was pulled out and put on the slide by using two wet cotton swabs. After that, a thin rectangular coverslip (24 mm × 32 mm) was put on the liver lobe and fixed by medical tapes to ensure that the coverslip was placed as horizontal as possible for water immersion objective. The coverslip should be in contact with the tissue without squeezing it.[32] ICG or CdSe/CdS/ZnS@SH-PEG2000 quantum dots were intravenously injected into the mouse right before imaging. 2TT-oC26B NPs were intravenously injected into the mouse 1 day before imaging.

2.3. *Experimental set up for measuring absorption spectrum and fluorescence spectrum*

The absorption spectrum of ICG in DMSO was measured by UV-VIS-NIR spectrophotometer (CARY 5000, Agilent). The fluorescence spectrum of ICG in DMSO was acquired by a home-built fluorescence spectra measurement system based on the PG2000 spectrometer (responsive to 370–1050 nm, Ideaoptics Instruments) and NIR2200 spectrometer (responsive to 900–2200 nm, Ideaoptics Instruments).

2.4. *Fiber-pinhole-based self-confocal NIR-II fluorescence microscope*

800 nm CW laser (Matisse; with continuously tunable single longitudinal mode; average output power @ 800 nm: 3 W; Spectra-Physics) beam was incident on the angle-adjustable reflective mirror for tuning the propagation direction. After reflected by

the mirror, laser beam passed through an 850 nm short-pass filter (FESH0850, Thorlabs) and a 950 nm short-pass dichroic mirror (DMSP950R, Thorlabs), and then was focused into the optical fiber by the singlet collimator (F220APC-1064, Thorlabs). After propagating in the optical fiber (MM-S105/125-22A, Connet Laser), laser reached the other end of fiber (optical fiber's core, diameter $= 105\,\mu$m), then collimated by the doublet collimator (F810APC-850, Thorlabs) again. Then, the collimated laser beam irradiated on the angle-adjustable reflective mirror, and was guided into a commercial scanning microscope (FV1200, Olympus). After that, the beam was reflected to the galvo–galvo scanning mirrors (scanning speed: $10\,\mu$s/pixel; scanning area: 512 pixels $\times 512$ pixels), which controlled the scanning process of laser focus in X–Y directions. Thereafter, the laser beam was expanded by a set of scan lens and tube lens, and eventually passed through the objective (XLPLN25XWMP2, $25\times$, NA $= 1.05$, Olympus) with near infrared anti-reflection coating and focused on the sample. NIR-II fluorescence excited by 800 nm CW laser from the sample traveled back roughly along the excitation path, and was refocused into the fiber-pinhole again. Propagating in the optical fiber and collimated by the singlet collimator, NIR-II fluorescence was then reflected by the 950 nm short-pass dichroic mirror (DMSP950R, Thorlabs) and passed through a 950 nm long-pass filter (FELH0950, Thorlabs). Finally, NIR-II fluorescence with wavelength longer than 950 nm was focused into an optical fiber by a collimator (F220APC-1064, Thorlabs) and propagated to the NIR (950–1700 nm) sensitive PMT (H12397-75, Hamamatsu). The electrical signal generated in the PMT was further amplified by an electrical signal amplifier (C12419, Hamamatsu), with synchronous signal from scanning galvanometer, to be transferred to the data acquisition card (NATIONAL INSTRUMENTS), based on which an image could be reconstructed via the computer.

2.5. *Fundamental air-pinhole-based self-confocal NIR-II fluorescence microscope*

800 nm fs pulsed laser (Mira-HP; repetition rate: 76 MHz; Coherent) beam was expanded by a pair of lenses, and then reflected by an angle-adjustable reflective mirror. Thereafter, the laser beam passed through an 850 nm short-pass filter (FESH0850, Thorlabs) and a 950 nm short-pass dichroic mirror (DMSP950R, Thorlabs), and then was focused into the aperture of a diaphragm (air-pinhole, aperture-adjustable) as the excitation focus by the pinhole-lens$_{\text{ex}}$ (AC254-030-B, Thorlabs). Followed by, the excitation focus was expanded by the pinhole-lens$_{\text{fl}}$ (AC254-030-B, Thorlabs), irradiating on the angle-adjustable reflective mirror, and was guided into the commercial scanning microscope (FV1200, Olympus). After reflected by the mirror, the laser beam was scanned by the galvo–galvo scanning mirror (scanning speed: $10\,\mu$s/pixel; scanning area: 512 pixels $\times 512$ pixels), which controlled the scanning process of laser focus in X–Y directions. Thereafter, the laser beam was expanded by a set of scan lens and tube lens, and eventually passed through the objective (XLPLN25XWMP2, $25\times$, NA $= 1.05$, Olympus) to be focused on the sample. NIR-II fluorescence excited by 800 nm fs pulsed laser from the sample traveled back roughly along the excitation path, and was refocused into the air-pinhole again by pinhole-lens$_{\text{fl}}$ (AC254-030-B, Thorlabs). Finally, collimated by the pinhole-lens$_{\text{ex}}$ (AC254-030-B, Thorlabs) and reflected by the 950 nm short-pass dichroic mirror (DMSP950R, Thorlabs), NIR-II fluorescence signal was detected by the NIR (950–1700 nm) sensitive PMT (H12397-75, Hamamatsu). The electrical signal generated in the PMT was further amplified by an electrical signal amplifier (C12419, Hamamatsu), with synchronous signal from scanning galvanometer, to be transferred to the data acquisition card (NATIONAL INSTRUMENTS), based on which a NIR-II fluorescence intensity image could be reconstructed via the computer.

2.6. *Air-pinhole-based self-confocal NIR-II fluorescence lifetime microscope*

800 nm fs pulsed laser (Mira-HP; repetition rate: 76 MHz; Coherent) beam was divided into two beams by a beam splitter at first. One weak beam reflected by the beam splitter was detected by a photodiode (PD) to synchronize the time location of laser pulse. The other strong beam's size was expanded by a pair of lenses after passing through the beam splitter, and then reflected by an angle-adjustable reflective mirror. Thereafter, the propagation paths of both the strong laser beam and the

NIR-II fluorescence signal were the same as those in *Fundamental air-pinhole-based self-confocal NIR-II fluorescence microscope.* After the NIR-II fluorescence signal was detected by the NIR (950–1700 nm) sensitive PMT (H12397-75, Hamamatsu), the time-correlated single-photon counting (TCSPC) module (SPC-150, Becker & Hickl GmbH) integrated in a computer would construct the NIR-II fluorescence lifetime confocal image according to the synchronous signals of laser pulses from PD and the galvo–galvo scanning mirrors, as well as electrical signals from a large-bandwidth responsive electrical amplifier (C5594, Hamamatsu) which amplified the signal from PMT.

2.7. *Air-pinhole-based self-confocal NIR-II fluorescence microscope integrated with multiphoton fluorescence microscopy*

The optical paths and signal processing of NIR-II fluorescence confocal microscope were the same as those in *Fundamental air-pinhole-based self-confocal NIR-II fluorescence microscope.* For multiphoton fluorescence microscopic imaging, the excitation path was the same as that in NIR-II fluorescence confocal microscopic imaging. The green multiphoton autofluorescence from liver excited by 800 nm fs pulsed laser was reflected by the 650 nm long-pass dichroic mirror (DMLP650R, Thorlabs), then passing through a band-pass filter (495–540 nm, Olympus), and was detected by a PMT (R3896, HAMAMATSU) responsive to visible light. The electrical signal generated in the PMT was processed by the commercial scanning microscope (FV1200, Olympus).

3. Results

3.1. *Fiber-pinhole-based self-confocal NIR-II fluorescence microscope*

The fiber-pinhole-based self-confocal NIR-II fluorescence microscope using the optical fiber core as the pinhole, is applicable to CW laser excitation (for fs laser, the normal optical fiber will broaden the dispersion), for obtaining the fluorescence intensity information of fluorophore (Fig. 1(a)). The optical fiber and the collimator in the dashed box (Fig. 1(a)) compose the self-confocal module (Fig. 1(b)). The excitation light (800 nm CW laser, displayed in blue) passing through the 950-nm short-pass dichroic mirror is focused on the optical fiber core by a singlet collimator, and then propagates to the optical fiber core at the other end (i.e., fiber-pinhole, diameter $= 105\,\mu$m) as the excitation focus. Afterwards, the excitation beam is collimated by a doublet collimator rather than a singlet collimator to reduce the chromatic dispersion, and then incidents on a reflective mirror. The reflected beam is scanned by the galvo–galvo scanning mirrors, and then passes through the scan lens, tube lens, as well as the objective to excite the fluorophore. Fluorescence from focus (displayed in pink) will roughly come back along the excitation path, and refocuses on the fiber-pinhole again, while most part of the out-of-focus fluorescence (displayed in green, Fig. 1(b)) will be filtered away by the fiber-pinhole. Finally, the fluorescence signal will be reflected by the dichroic mirror and be collected by the PMT. This process is automatic and adjustment-free, providing a more convenient access to researchers.

We used this system to image cerebral vessels of intravital mice which were intravenously injected with ICG. ICG's absorption peak is around 800 nm, and its fluorescence spectrum tails beyond 950 nm (Fig. S1). Diameters of vessels, calculated by the full width half maximums (FWHMs) along the white dotted lines at $200\,\mu$m, $350\,\mu$m and $550\,\mu$m depths below the pial surface of the cortex (Fig. 1(c)), are $4.7\,\mu$m, $3.4\,\mu$m and $4.7\,\mu$m, respectively. The imaging depth can reach $\sim 700\,\mu$m (Fig. S2). Compared to traditional NIR-II fluorescence confocal microscope equipped with the same PMT (600 V) and comparable pinhole diameter ($150\,\mu$m), the temporal resolution and the excitation power of fiber-pinhole-based self-confocal NIR-II fluorescence microscope is much better ($10\,\mu$s/pixel $<< 3.3$ ms/pixel, 25 mW < 40 mW) with similar imaging depth in the substantive tissue ($\sim 700\,\mu$m).[33] Meanwhile, in contrast to cerebrovascular imaging of the mouse injected with DCBT nanoparticles (NPs)[30] performed by multiphoton fluorescence microscope under 800 nm fs excitation (Fig. S3), whose imaging depth is $\sim 550\,\mu$m and spatial resolution is $\sim 2.8\,\mu$m at $500\,\mu$m depth (Fig. S4), the fiber-pinhole-based self-confocal NIR-II fluorescence microscopy with 800 nm CW excitation enables larger imaging depth under similar imaging conditions, and thus proving that it can replace multiphoton microscopy in some cases with lower cost and much better biological friendliness.
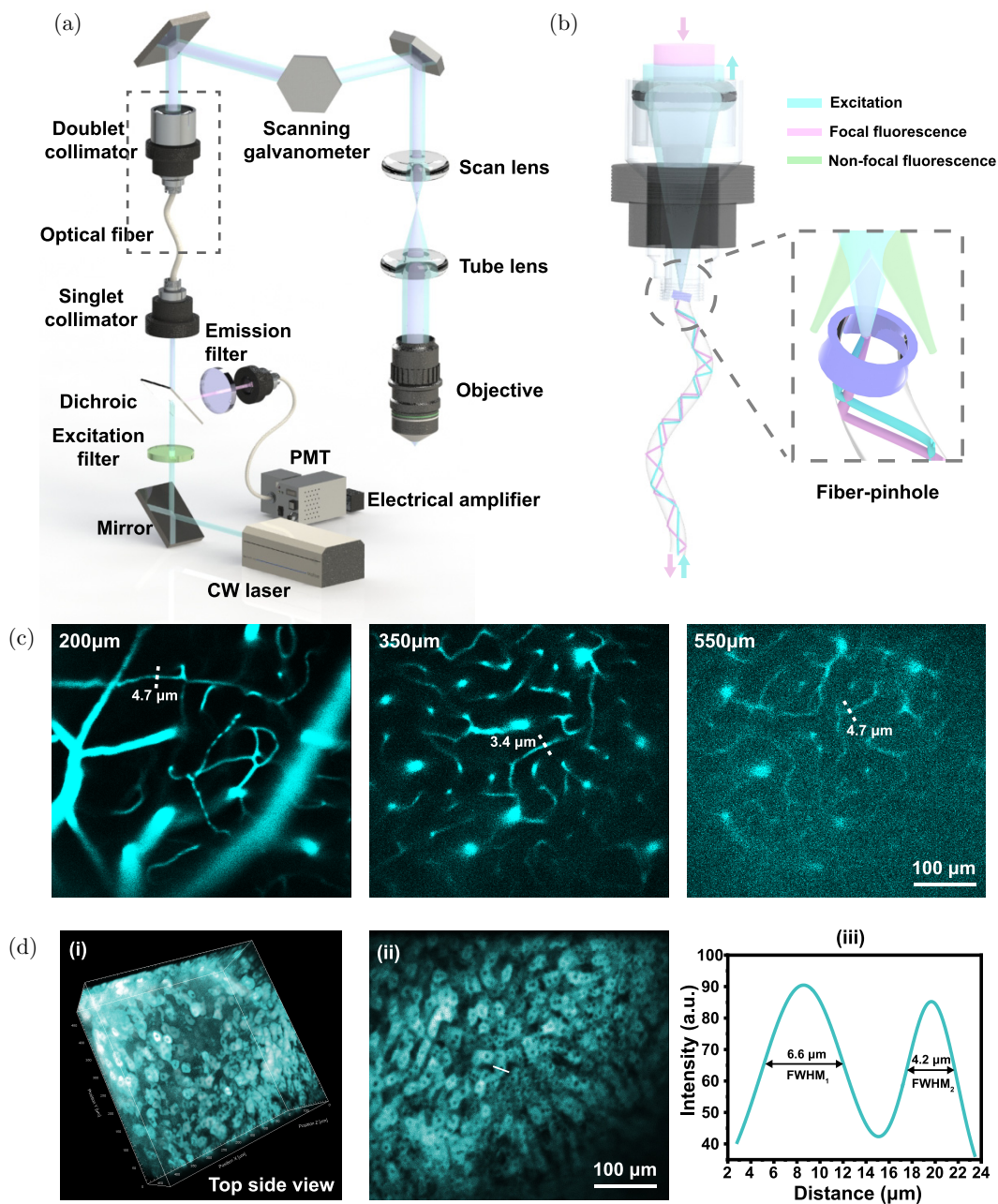
Fig. 1. Fiber-pinhole-based self-confocal NIR-II fluorescence microscope for cerebrovascular and hepatocellular imaging. (a) Schematic of fiber-pinhole-based self-confocal NIR-II fluorescence microscope. (b) Magnified self-confocal module framed by the dashed box in (a) and its working principle. (c) Cerebrovascular images of the mouse at various depths ($200\,\mu$m, $350\,\mu$m and $550\,\mu$m) below the pial surface. The mouse was injected with ICG ($5\,$mg/mL, $200\,\mu$L). Excitation: $800\,$nm CW laser ($25\,$mW under objective); fluorescence collection band: $> 950\,$nm; scanning speed: $10\,\mu$s/pixel, PMT voltage: $500\,$V. Scale bar: $100\,\mu$m. (d) Hepatocyte images of the mouse. (i) Top side view of hepatocellular 3D reconstructed image. (ii) The hepatocyte image at one depth of the mouse's liver. (iii) The intensity distribution along the white line on a hepatocyte taking in ICG in (ii) and the corresponding FWHM analysis. The mouse was injected with ICG ($5\,$mg/mL, $200\,\mu$L). Excitation: $800\,$nm CW laser ($2\,$mW under objective); fluorescence collection band: $> 950\,$nm; scanning speed: $10\,\mu$s/pixel, PMT voltage: $450\,$V. Scale bar: $100\,\mu$m.

Although the fiber-pinhole-based self-confocal NIR-II fluorescence microscope for imaging vessels is commendable, the excitation power ($25\,$mW) under the objective is still highly expected to be decreased. That's because the metabolism of ICG in the blood vessels is too rapid (half-life time $< 10\,$min)[1,34,35] to retain a sufficient concentration for vascular imaging, the excitation power

needs to increase accordingly to compensate the decreased concentration of ICG. Since ICG is metabolized by digestive system, it will be continuously ingested and released by hepatocytes at the same time, which maintains a stable concentration of ICG in the hepatocyte within a long-term (several hours) experiment. Without the concern of rapid decline of ICG's concentration in hepatocytes, we used this system to image hepatocytes of the intravital mice intravenously injected with ICG. The results show that hepatocytes can be clearly imaged with narrow tomography by the fiber-pinhole-based self-confocal NIR-II fluorescence microscope under extremely low excitation power (2 mW under the objective, this is the lowest excitation power according to the published literatures) (Fig. 1 (d)(ii)). It can be seen that cytoplasm and nucleus are clearly identified. The intensity distribution along the white line on the hepatocyte in Fig. 1(d) (ii) is shown in Fig. 1(d)(iii). The complete cell's width is $\sim 20\,\mu$m. FWHMs of the two peaks represent the widths of cytoplasm separated by the nucleus, which are $6.6\,\mu$m and $4.2\,\mu$m, respectively. According to previous studies, light scattering coefficient of liver is ~ 7 times as much as that of the brain,[36–38] hence the total imaging depth of hepatocytes (184 μm) is less than that of brain, but ~ 2 times deeper than traditional visible fluorescence confocal microscopy.[39] The 3D reconstruction of hepatocytes near the surface of liver is shown as top side view (Fig. 1(d)(i)). It is thus indisputably clear that the fiber-pinhole-based self-confocal NIR-II fluorescence microscope improves the confocal efficiency to a great extent.

3.2. *Air-pinhole-based self-confocal NIR-II fluorescence microscopy*

Even though the fiber-pinhole-based self-confocal NIR-II fluorescence microscope with CW laser excitation has outstanding advantages for fluorescence imaging, some specific applications like fluorescence lifetime imaging that have to use fs pulsed laser excitation are still not satisfied by it. Therefore, the need to build a self-confocal NIR-II fluorescence microscope which is suitable for fs laser excitation is imminent. An air-pinhole-based self-confocal NIR-II fluorescence microscope using a diaphragm with continuously adjustable aperture as the pinhole is designed and established in our work

(Fig. 2(a)). Since there is no fiber in the excitation path, it can be definitely applicable to fs pulsed laser excitation to record fluorescence lifetime information. In addition, multi-color information can also be obtained if it is combined with multiphoton fluorescence microscopy.

3.2.1. *Fundamental air-pinhole-based self-confocal NIR-II fluorescence microscope*

Fundamental air-pinhole-based self-confocal NIR-II fluorescence microscope is shown in Fig. 2(a). Pinhole-lens$_{ex}$, air-pinhole and pinhole-lens$_{fl}$ in the dashed box of Fig. 2(a) compose the crucial part, self-confocal module (magnified in Fig. 2(b)). After passing through the 950 nm short-pass dichroic mirror and being focused on the air-pinhole as the excitation focus by pinhole-lens$_{ex}$, the excitation light (800 nm fs laser, displayed in blue) is then expanded by pinhole-lens$_{fl}$ and afterwards incidents on the reflective mirror. Subsequently, the laser beam scans the sample in X–Y directions by galvo–galvo scanning mirrors after passing through the scan lens, tube lens and objective. Afterwards, the NIR-II fluorescence (displayed in pink) from the focus in the sample will roughly come back along the excitation path, and refocuses on the air-pinhole again, while most part of the out-of-focus fluorescence (displayed in green, Fig. 2(b)) will be filtered away by the air-pinhole. Lastly, the NIR-II fluorescence signal will be reflected by the dichroic mirror and collected by the PMT. Although this system needs to be adjusted (make the excitation focus locate inside the air-pinhole), the adjustment process can be controlled as planned. First of all, translate the pinhole-lens$_{ex}$ along the optical axis to focus the excitation light onto the air-pinhole plane. Then adjust the incidence angle of excitation light to make the excitation focus locate inside the air-pinhole. Finally, translate the excitation light to align it with the optical axis of the system. Besides, the operation is simple, since the strong excitation light can be easily observed. It is more convenient and time-saving than adjusting traditional NIR-II fluorescence confocal microscope.

We used this system to carry out fundamental intensity imaging of cerebral vessels of intravital mice which were intravenously injected with ICG. The imaging result with wonderfully abundant
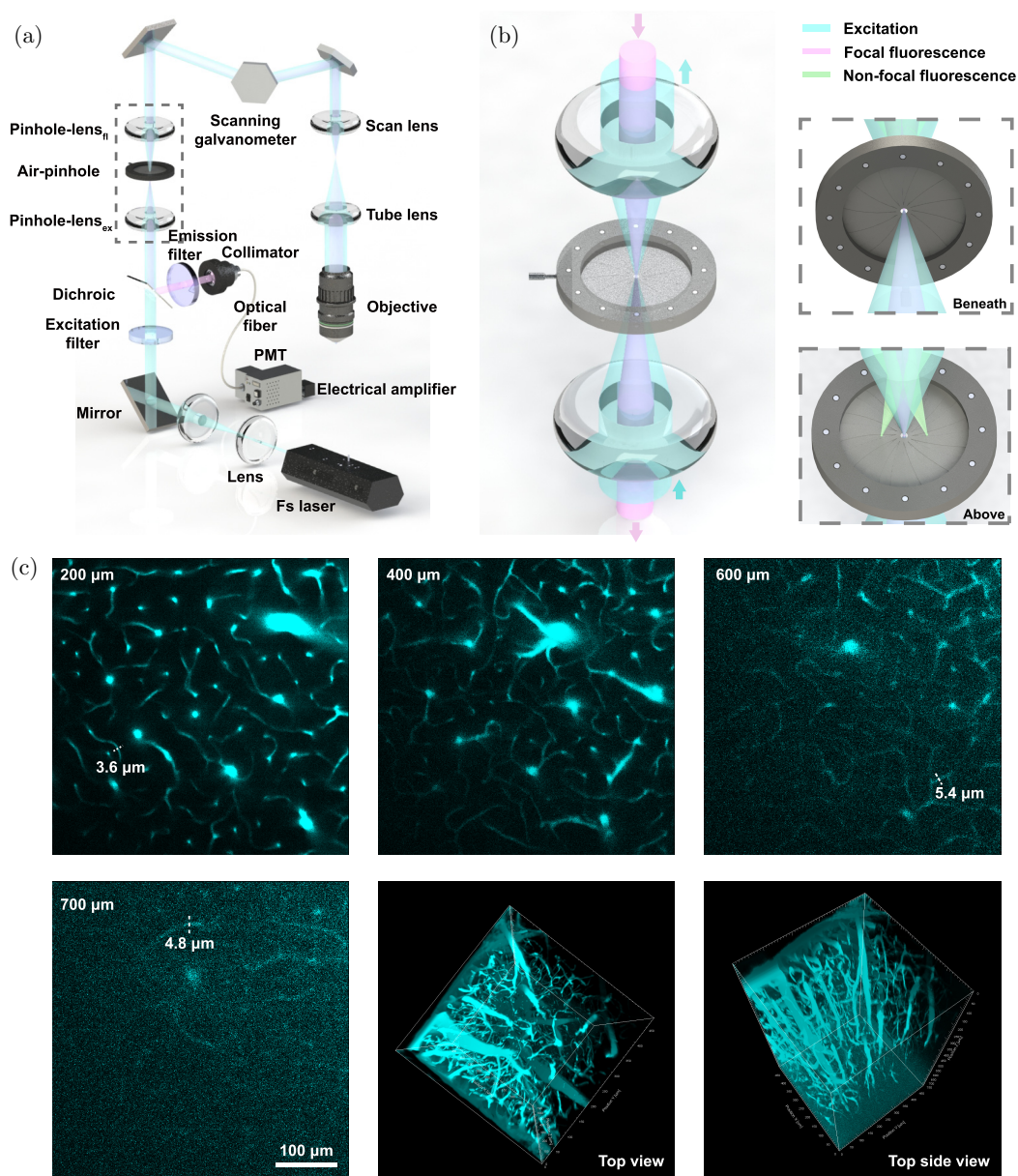
Fig. 2. Fundamental air-pinhole-based self-confocal NIR-II fluorescence microscope for cerebrovascular imaging. (a) Schematic of fundamental air-pinhole-based self-confocal NIR-II fluorescence microscope. (b) Magnified self-confocal module framed by the dashed box in (a) and its working principle. (c) NIR-II fluorescence intensity images of mouse's cerebral vessels at various depths below the pial surface (from $200\,\mu$m to $700\,\mu$m). Top view and top side view of cerebrovascular 3D reconstruction are shown (from $0\,\mu$m to $760\,\mu$m). The mouse was injected with ICG (5 mg/mL, 200 μL). Excitation: 800 nm fs pulsed laser ($30\,$mW under objective); fluorescence collection band: $> 950\,$nm; pinhole aperture: $200\,\mu$m; scanning speed: $10\,\mu$s/pixel; PMT voltage: $600\,$V. Scale bar: $100\,\mu$m.

cerebral vessels is presented in Fig. 2(c). The imaging depth reaches $\sim 760\,\mu$m. Diameters of cerebral vessels marked by white dotted lines at $200\,\mu$m, $600\,\mu$m and $700\,\mu$m depths are $3.6\,\mu$m, $5.4\,\mu$m and $4.8\,\mu$m, respectively. The 3D reconstructions of cerebral vessels by top view and top side view are displayed in Fig. 2(c).

3.2.2. *Air-pinhole-based self-confocal NIR-II fluorescence lifetime microscopy*

Different structures labeled with different fluorophores can be distinguished by different fluorescence lifetimes of fluorophores within the same detected spectral region. With fs pulsed laser excitation and TCSPC module, air-pinhole-based

self-confocal NIR-II fluorescence lifetime microscope is able to measure the fluorescence lifetime of fluorophore (Fig. S5). First of all, fluorescence lifetimes of two fluorophores, ICG and 2TT-oC26B NPs,[31] were measured *in vitro*. With numerous fluorescent photons collected from ICG (photon count = 2822) and 2TT-oC26B NPs (photon count = 961, 317), the fluorescence lifetime of ICG is calculated as $\sim 689\,\text{ps}$, while that of 2TT-oC26B NPs is $\sim 404\,\text{ps}$. These two lifetimes are significantly different (Fig. 3(a)). In order to know the accurate distributions and fluorescence lifetimes of ICG and 2TT-oC26B NPs in mouse, as references, we preliminarily injected ICG or 2TT-oC26B NPs into two similar C57BL/6 mice individually in the same way, and then performed fluorescence lifetime
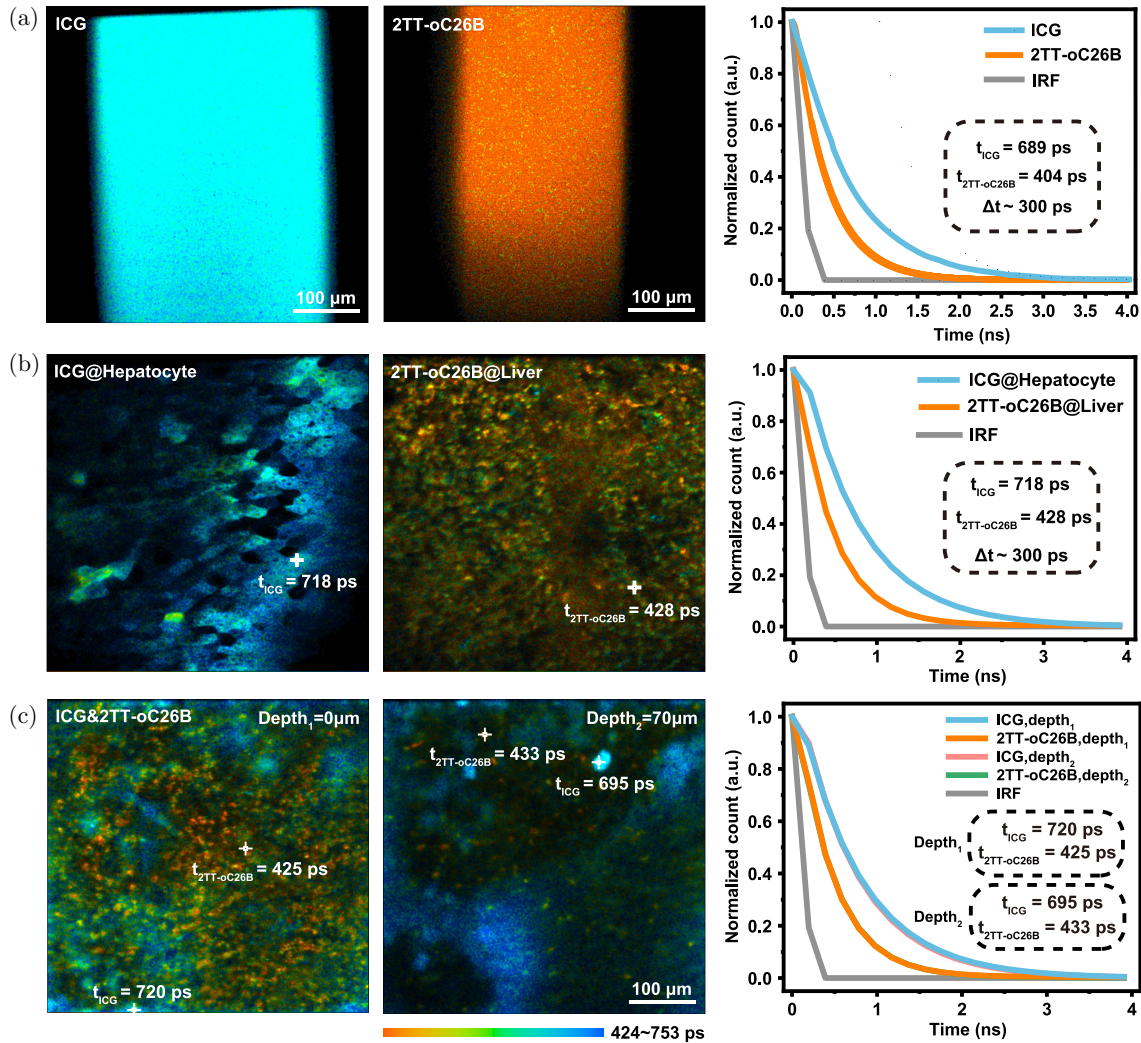

Fig. 3. Air-pinhole-based self-confocal NIR-II fluorescence lifetime microscope for distinguishing different hepatic structures by diverse fluorescence lifetimes. (a) Fluorescence lifetime images and decay curves (with calculated fluorescence lifetimes) of ICG (displayed in blue) and 2TT-oC26B NPs (displayed in orange) *in vitro*. (b) Fluorescence lifetime images of hepatocytes of a mouse intravenously injected with ICG (1 mg/ml, 100 μL) and of other hepatic components of the other mouse intravenously injected with 2TT-oC26B NPs (2 mg/ml, 100 μL). Fluorescence decay curves (with calculated fluorescence lifetimes) of ICG in hepatocytes (displayed in blue) and 2TT-oC26B NPs in other hepatic components (displayed in orange), which are marked with white crosses in fluorescence lifetime images, are attached. (c) Fluorescence lifetime images of hepatocytes (blue) and other hepatic components (orange) at two focusing depths (depth$_1$ = 0 μm, depth$_2$ = 70 μm) in the liver of a mouse intravenously injected with both ICG (1 mg/ml, 100 μL) and 2TT-oC26B NPs (2 mg/ml, 100 μL). Fluorescence decay curves (with calculated fluorescence lifetimes) of ICG in hepatocytes and 2TT-oC26B NPs in other hepatic components at focusing depth$_1$ and depth$_2$ (both marked with white crosses in fluorescence lifetime images) are attached. Instrument response function (IRF) is $\sim 154\,\text{ps}$. Excitation: 800 nm fs pulsed laser (2 mW under objective); fluorescence collection band: $> 950\,\text{nm}$; pinhole aperture: 200 μm; scanning speed: 10 μs/pixel; PMT voltage: 500 V. Scale bar: 100 μm.

microscopic imaging. Results show that ICG is taken up by hepatocytes (blue) and enriched in them with the fluorescence lifetime of $\sim 700\,$ps, while 2TT-oC26B NPs spread over other hepatic components (orange) with the fluorescence lifetime of $\sim 400\,$ps (Fig. 3(b)). Fluorescence lifetimes of ICG and 2TT-oC26B NPs *in vivo* are consistent with the *in vitro* results as wondering. Finally, we injected ICG and 2TT-oC26B NPs together to the same mouse. With only one collected fluorescence spectral band ($> 950\,$nm) and one PMT, hepatocytes taking in ICG (blue) and other hepatic components stained by 2TT-oC26B NPs (orange) at two focusing depths ($\text{depth}_1 = 0\,\mu$m, $\text{depth}_2 = 70\,\mu$m) can be clearly distinguished by different fluorescence lifetimes (ICG, $\sim 700\,$ps; 2TT-oC26B NPs, $\sim 400\,$ps) successfully (Fig. 3(c)). The corresponding fluorescence intensity images to Figs. 3(b) and 3(c) can be seen in Fig. S6. Although there was the multi-channel NIR-II fluorescence lifetime confocal microscopy for the mouse ear *in vivo* imaging,[40] which adopted the traditional confocal optical path and used the superconducting single-photon detector (SSPD) as the detector with high sensitivity to NIR-II signals (detection efficiency $> 50\%$), our work is still the first demonstration of self-confocal multi-channel NIR-II fluorescence lifetime microscopy for the liver, which has high scattering coefficient, of the intravital mouse by using low detection efficiency ($\sim 2\%$) PMT with considerable confocal efficiency (extremely low excitation power: $2\,$mW under objective), being a pilot study as well as a positive exploration. These results prove that air-pinhole-based self-confocal NIR-II fluorescence lifetime microscope is a promising technology for implementing multi-structure imaging, and it will further facilitate the study on the *in vivo* distribution and metabolism of various NIR-II fluorophores in both biological researches and clinical trials.

3.2.3. *Air-pinhole-based self-confocal NIR-II fluorescence microscope integrated with multiphoton fluorescence microscopy*

Multiphoton fluorescence microscope with multiple detection channels responding to different spectral bands (such as blue, green and red channels) is used to observe multiple structures (e.g., myelin, neurons and blood vessels) specifically labeled by mature fluorophores in abundant supply with different fluorescence peaks, and has been widely used in neuroscience, immunology, etc.[41–43] However, the quantity of detection channels in multi-color multiphoton fluorescence microscope for simultaneously observing multiple structures is still constrained for avoiding fluorescence cross-talk, because of the broad fluorescence spectra of commonly used fluorophores. A wise move for extending imaging channels is to introduce single-photon excited down-conversion fluorescence confocal microscopy into multiphoton excited up-conversion fluorescence microscopy (Fig. 4(a)), to further increase the application potential in certain areas such as neuroscience.

In this work, we used a single $800\,$nm fs pulsed laser to simultaneously excite multiphoton up-conversion autofluorescence of mouse's liver and single-photon down-conversion NIR-II fluorescence of ICG in hepatocytes as a preliminary demo (Fig. 4(b)). The physical principle is shown in Fig. 4(a). Benefiting from the air-pinhole of self-confocal-based NIR-II fluorescence microscope (Fig. S7), the pulse width of fs laser won't be broadened after passing through the pinhole, and thus can excite multiphoton fluorescence with sufficient brightness. Green multiphoton autofluorescence of the liver will be reflected by the $650\,$nm long-pass dichroic mirror ($\text{Dichroic}_{\text{MP}}$) and collected by the PMT_{MP} responsive to the visible light. Meanwhile, NIR-II fluorescence of ICG in hepatocytes excited by $800\,$nm fs pulsed laser will pass through the $650\,$nm long-pass dichroic mirror and finally collected by the $\text{PMT}_{\text{NIR–II}}$ responsive to NIR-II light. Consequently, multi-color microscopic imaging (up-conversion and down-conversion) of different hepatic structures under single fs pulsed excitation can be achieved. The dispersed spotted components at one area of the liver of the mouse generate green multiphoton autofluorescence under $800\,$nm fs pulsed excitation (Fig. 4(c)). After intravenously injecting ICG into the mouse, we can see the NIR-II fluorescence confocal microscopic image of wedge-shaped hepatocytes in this area. In another area distributed with hepatocyte cords (recognized by the bright NIR-II fluorescence signal in this area, Fig. 4(d)), there still are many same components as in Fig. 4(c) generating green multiphoton autofluorescence (Fig. 4(d)). Fusion images of dispersed spotted components and hepatocytes (Figs. 4(c) and 4(d)) indicate that the specific hepatic components
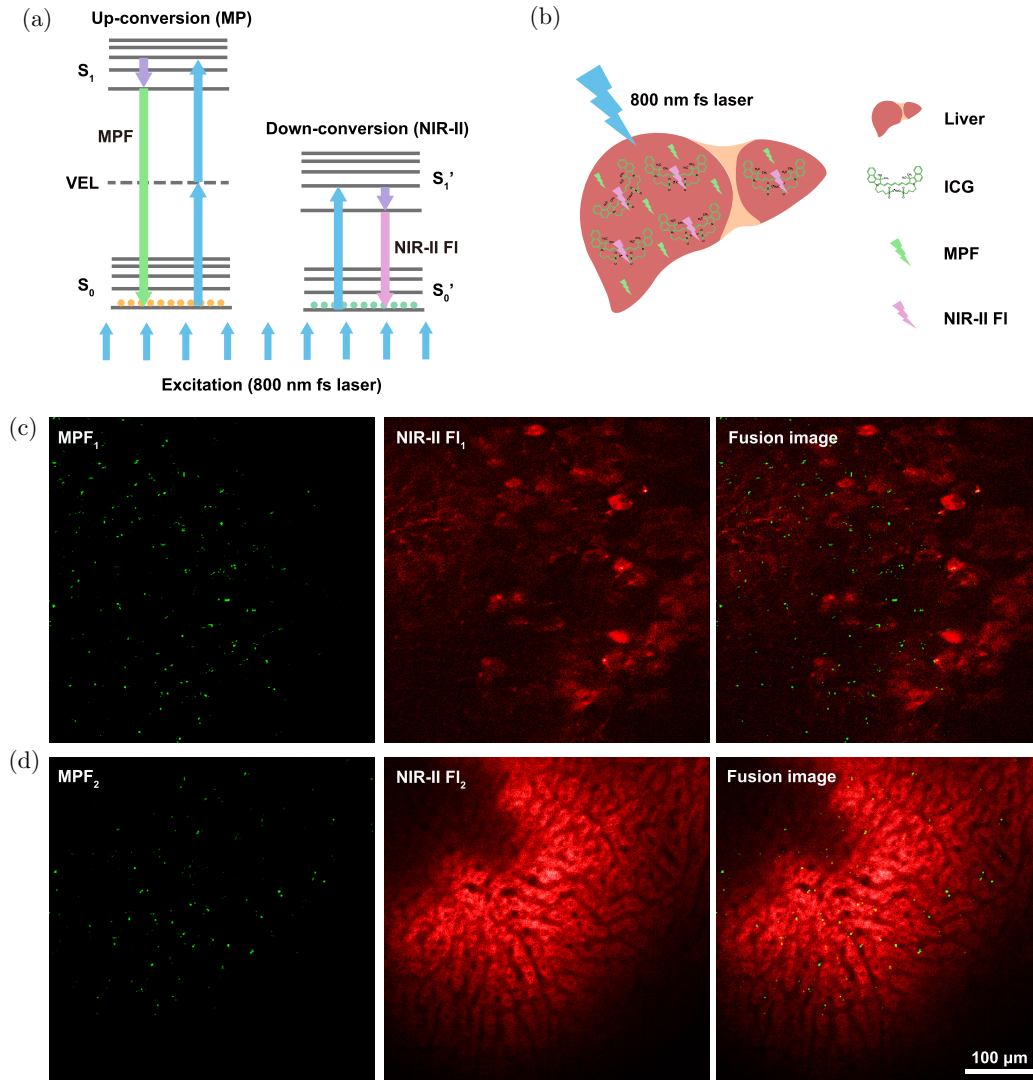
Notes: MPF — multiphoton fluorescence; NIR-II Fl — NIR-II fluorescence.

Fig. 4. Air-pinhole-based self-confocal NIR-II fluorescence microscope integrated with multiphoton microscopy for hepatic structure multi-color imaging. (a) Physical principle and energy level transitions of multi-color microscopic imaging (up-conversion and down-conversion) under single 800 nm fs pulsed laser excitation. (b) ICG in hepatocytes emit NIR-II fluorescence (pink arrow) and intrinsic hepatic components emit multiphoton autofluorescence (green arrow) under 800 nm fs pulsed laser excitation (blue arrow). (c) Multiphoton autofluorescence microscopic imaging (MPF$_1$) of intrinsic hepatic components and NIR-II fluorescence confocal microscopic imaging (NIR-II Fl$_1$) of wedge-shaped hepatocytes in one area of the liver of the mouse injected with ICG (1 mg/ml, 100 μL), as well as fusion image of MPF$_1$ and NIR-II Fl$_1$ for visualizing the relative position of intrinsic hepatic components and wedge-shaped hepatocytes in this area. (d) Multiphoton autofluorescence microscopic imaging (MPF$_2$) of intrinsic hepatic components in the area distributed with hepatocyte cords and NIR-II fluorescence confocal microscopic imaging (NIR-II Fl$_2$) of hepatocyte cords of the mouse injected with ICG (1 mg/ml, 100 μL), as well as fusion image of MPF$_2$ and NIR-II Fl$_2$ for visualizing the relative position of intrinsic hepatic components and hepatocyte cords. Excitation: 800 nm fs pulsed laser (1 mW for NIR-II fluorescence confocal microscopic imaging under objective, 15 mW for multiphoton fluorescence microscopic imaging under objective); fluorescence collection band: ($>$ 950 nm for NIR-II fluorescence confocal imaging, 495–540 nm for multiphoton fluorescence imaging); pinhole aperture: 200 μm; scanning speed: 10 μs/pixel; PMT voltage: 600 V. Scale bar: 100 μm.

generating green multiphoton autofluorescence mainly locate in the gap between hepatocytes. We then performed the multiphoton imaging of hepatic sinusoids (blood in the liver, Fig. S8) of another mouse. The result shows that the spots (green channel) almost all locate in the hepatic sinusoids (the gap between hepatocytes, orange channel). So the spots may be bile acids, immune cells, etc., in

the hepatic sinusoids. The multiphoton microscopic imaging of intrinsic hepatic components (green channel, 495–540 nm) at different depths ($80\,\mu$m, $120\,\mu$m and $160\,\mu$m) of the mouse under 800 nm fs excitation are showed in Fig. S9. The multiphoton microscopic imaging of intrinsic hepatic components (red channel, > 700 nm) of another blank mouse under 1700 nm fs laser excitation is shown in Fig. S10.

Exerting more efficient excitation (1 mW under objective) and collection of NIR-II fluorescence signals, air-pinhole-based self-confocal NIR-II fluorescence microscope integrated with multiphoton fluorescence microscopy further extends the imaging channels, providing another technical support for multifunctional imaging studies in fields such as neuroscience.

4. Discussion

The self-confocal NIR-II fluorescence microscopy with the advantages of high confocal efficiency leading to extremely low excitation power, free/easily adjustment, large imaging depth and multifunction, is extraordinary attractive. Fiber-pinhole-based self-confocal NIR-II fluorescence microscope applicable to CW laser excitation can be used for normal fluorescence intensity imaging to observe biological structures, for example, cerebrovascular imaging, hepatocyte imaging, etc. Air-pinhole-based self-confocal NIR-II fluorescence microscope applicable to fs pulsed laser excitation can be used not only for basic fluorescence intensity imaging, but also for multi-channel fluorescence lifetime imaging. As for air-pinhole-based self-confocal NIR-II fluorescence microscope combined with multiphoton fluorescence microscopy, it provides more color channels for observing a variety of biological structures simultaneously.

Self-confocal NIR-II fluorescence microscopes still have plenty room for improvement. Replacing PMT with SNSPD, which is much more sensitive to photons and responsive to longer wavelength than PMT, self-confocal NIR-II fluorescence microscopy can be applicable to longer-wavelength excitation, like 1300 nm fs laser, for detecting longer-wavelength fluorescence with much higher efficiency, and greatly improve the imaging depth and speed. Adaptive optics for correcting excitation beam's wavefront, which promotes excitation light to penetrate deeper and focus tighter in the biological tissues,

also can be introduced into the self-confocal NIR-II fluorescence microscopes to improve the imaging depth and resolution.

With anticipation, since the fluorescence lifetime can reflect fluorophore's concentration, polarity and viscosity, which are affected by the environment,[44] multi-channel NIR-II fluorescence lifetime microscopic imaging is a powerful tool for studying metabolism of a variety of endogenous substances, and evaluating pharmacokinetics and biosafety of multiple exogenous probes *in vivo*. What's more, multi-channel NIR-II fluorescence lifetime imaging and multi-color fluorescence imaging can be integrated together to implement multi-plus-channel and multi-functional imaging in the future. These systems will effectively provide larger platforms for biomedical researches, and thus significantly promote the biomedical field.

5. Conclusions

We developed the fiber-pinhole-based self-confocal NIR-II fluorescence microscope for fluorescence intensity imaging to observe biological structures. For further multifunctional imaging, we developed the air-pinhole-based self-confocal NIR-II fluorescence microscope for multi-channel fluorescence lifetime imaging and multi-color imaging. With free/easily adjustment, high confocal efficiency, large imaging depth and multifunction, these systems are expected to be widely used in the field of biomedical research.

Acknowledgment

Conflicts of Interest

The authors declare the following financial interests/personal relationships which may be considered as potential competing interests: Jun Qian has patent #ZL 2020 1 1607103.6 licensed to Zhejiang University.

Supporting Information

The material is available at https://www.worldscientific.com/doi/suppl/10.1142/S1793545823500256

ORCID

Jing Zhou ⓘ https://orcid.org/0000-0002-3269-601X
Tianxiang Wu ⓘ https://orcid.org/0000-0003-0778-0380
Runze Chen ⓘ https://orcid.org/0000-0002-1697-2934
Yifei Li ⓘ https://orcid.org/0009-0009-1059-9268

References

1. T. Ishizawa, N. Fukushima, J. Shibahara, K. Masuda, S. Tamura, T. Aoki, K. Hasegawa, Y. Beck, M. Fukayama, N. Kokudo, "Real-time identification of liver cancers by using indocyanine green fluorescent imaging," *Cancer* **115**(11), 2491–2504 (2009).

2. B. Zhu, E. M. Sevick-Muraca, "A review of performance of near-infrared fluorescence imaging devices used in clinical studies," *Br. J. Radiol.* **88**(1045), 20140547 (2015).

3. Z. Hu, C. Fang, B. Li, Z. Zhang, C. Cao, M. Cai, S. Su, X. Sun, X. Shi, C. Li, T. Zhou, Y. Zhang, C. Chi, P. He, X. Xia, Y. Chen, S. S. Gambhir, Z. Cheng, J. Tian, "First-in-human liver-tumour surgery guided by multispectral fluorescence imaging in the visible and near-infrared-I/II windows," *Nat. Biomed. Eng.* **4**(3), 259–271 (2020).

4. J. Zhou, X. Fan, D. Wu, J. Liu, Y. Zhang, Z. Ye, D. Xue, M. He, L. Zhu, Z. Feng, A. N. Kuzmin, W. Liu, P. N. Prasad, J. Qian, "Hot-band absorption of indocyanine green for advanced anti-stokes fluorescence bioimaging," *Light Sci. Appl.* **10**(1), 182 (2021).

5. Y. Li, X. Fan, Y. Li, L. Zhu, R. Chen, Y. Zhang, H. Ni, Q. Xia, Z. Feng, B. Z. Tang, J. Qian, H. Lin, "Biologically excretable AIE nanoparticles wear tumor cell-derived "exosome caps" for efficient NIR-II fluorescence imaging-guided photothermal therapy," *Nano Today* **41**, 101333 (2021).

6. P. Tolar, H. W. Sohn, S. K. Pierce, "The initiation of antigen-induced B cell antigen receptor signaling viewed in living cells by fluorescence resonance energy transfer," *Nat. Immunol.* **6**(11), 1168–1176 (2005).

7. M. Chalfie, Y. Tu, G. Euskirchen, W. W. Ward, D. C. Prasher, "Green fluorescent protein as a marker for gene expression," *Science* **263**(5148), 802–805 (1994).

8. L. M. Smith, J. Z. Sanders, R. J. Kaiser, P. Hughes, C. Dodd, C. R. Connell, C. Heiner, S. b. H. Kent, L. E. Hood, "Fluorescence detection in automated DNA sequence analysis," *Nature* **321**(6071), 674–679 (1986).

9. P. A. Summers, B. W. Lewis, J. Gonzalez-Garcia, R. M. Porreca, A. H. M. Lim, P. Cadinu, N. Martin-Pintado, D. J. Mann, J. B. Edel, J. B. Vannier, M. K. Kuimova, R. Vilar, "Visualising G-quadruplex DNA dynamics in live cells by fluorescence lifetime imaging microscopy," *Nat. Commun.* **12**(1), 162 (2021).

10. Y. Yu, J. Yu, Z. L. Huang, F. Zhou, "Application of super-resolution fluorescence microscopy in hematologic malignancies," *J. Innov. Opt. Health Sci.* **15**(2), 2230005 (2022).

11. J. Liao, J. Qu, Y. Hao, J. Li, "Deep-learning-based methods for super-resolution fluorescence microscopy," *J. Innov. Opt. Health Sci.* **16**, 2230016 (2022).

12. K. Wang, S. Tang, S. Wang, F. Lin, G. Zou, J. Qu, L. Liu, "Monitoring microenvironment of Hep G2 cell apoptosis using two-photon fluorescence lifetime imaging microscopy," *J. Innov. Opt. Health Sci.* **15**(3), 2250014 (2022).

13. L. Tian, S. A. Hires, T. Mao, D. Huber, M. E. Chiappe, S. H. Chalasani, L. Petreanu, J. Akerboom, S. A. McKinney, E. R. Schreiter, C. I. Bargmann, V. Jayaraman, K. Svoboda, L. L. Looger, "Imaging neural activity in worms, flies and mice with improved GCaMP calcium indicators," *Nat. Methods* **6**(12), 875–881 (2009).

14. E. B. Brown, R. B. Campbell, Y. Tsuzuki, L. Xu, P. Carmeliet, D. Fukumura, R. K. Jain, "*In vivo* measurement of gene expression, angiogenesis and physiological function in tumors using multiphoton laser scanning microscopy," *Nat. Med.* **7**(7), 864–868 (2001).

15. W. Wang, J. B. Wyckoff, V. C. Frohlich, Y. Oleynikov, S. Hüttelmaier, J. Zavadil, L. Cermak, E. P. Bottinger, R. H. Singer, J. G. White, J. E. Segall, J. S. Condeelis, "Single cell behavior in metastatic primary mammary tumors correlated with gene expression patterns revealed by molecular profiling," *Cancer Res.* **62**(21), 6278–6288 (2002).

16. M. J. Miller, S. H. Wei, I. Parker, M. D. Cahalan, "Two-photon imaging of lymphocyte motility and antigen response in intact lymph node," *Science* **296**(5574), 1869–1873 (2002).

17. J. M. Squirrell, D. L. Wokosin, J. G. White, B. D. Bavister, "Long-term two-photon fluorescence imaging of mammalian embryos without compromising viability," *Nat. Biotechnol.* **17**(8), 763–767 (1999).

18. A. Vogel, J. Noack, G. H'uttman, G. Paltauf, "Mechanisms of femtosecond laser nanosurgery of cells and tissues," *Appl. Phys. B* **81**(8), 1015–1047 (2005).

19. K. Welsher, S. P. Sherlock, H. Dai, "Deep-tissue anatomical imaging of mice using carbon nanotube fluorophores in the second near-infrared window," *Proc. Natl. Acad. Sci. U.S.A.* **108**(22), 8943–8948 (2011).

20. N. G. Horton, K. Wang, D. Kobat, C. G. Clark, F. W. Wise, C. B. Schaffer, C. Xu, "*In vivo* three-photon microscopy of subcortical structures within an intact mouse brain," *Nat. Photon.* **7**(3), 205–209 (2013).

21. D. Wu, D. Xue, J. Zhou, Y. Wang, Z. Feng, J. Xu, H. Lin, J. Qian, X. Cai, "Extrahepatic cholangiography in near-infrared II window with the clinically approved fluorescence agent indocyanine green: a promising imaging technology for intraoperative diagnosis," *Theranostics* **10**(8), 3636–3651 (2020).

22. Z. Feng, T. Tang, T. Wu, X. Yu, Y. Zhang, M. Wang, J. Zheng, Y. Ying, S. Chen, J. Zhou, X. Fan, D. Zhang, S. Li, M. Zhang, J. Qian, "Perfecting and extending the near-infrared imaging window," *Light Sci. Appl.* **10**(1), 197 (2021).

23. Z. Feng, S. Bai, J. Qi, C. Sun, Y. Zhang, X. Yu, H. Ni, D. Wu, X. Fan, D. Xue, S. Liu, M. Chen, J. Gong, P. Wei, M. He, J. W. Y. Lam, X. Li, B. Z. Tang, L. Gao, J. Qian, "Biologically excretable aggregation-induced emission dots for visualizing through the marmosets intravitally: horizons in future clinical nanomedicine," *Adv. Mater.* **33**(17), e2008123 (2021).

24. S. Zhu, S. Herraiz, J. Yue, M. Zhang, H. Wan, Q. Yang, Z. Ma, Y. Wang, J. He, A. L. Antaris, Y. Zhong, S. Diao, Y. Feng, Y. Zhou, K. Yu, G. Hong, Y. Liang, A. J. Hsueh, H. Dai, "3D NIR-II molecular imaging distinguishes targeted organs with high-performance NIR-II bioconjugates," *Adv. Mater.* **30**(13), e1705799 (2018).

25. W. Yu, B. Guo, H. Zhang, J. Zhou, X. Yu, L. Zhu, D. Xue, W. Liu, X. Sun, J. Qian, "NIR-II fluorescence *in vivo* confocal microscopy with aggregation-induced emission dots," *Sci. Bull. (Beijing)* **64**(6), 410–416 (2019).

26. Z. Cai, L. Zhu, M. Wang, A. W. Roe, W. Xi, J. Qian, "NIR-II fluorescence microscopic imaging of cortical vasculature in non-human primates," *Theranostics* **10**(9), 4265–4276 (2020).

27. X. Fan, Y. Li, Z. Feng, G. Chen, J. Zhou, M. He, L. Wu, S. Li, J. Qian, H. Lin, "Nanoprobes-assisted multichannel NIR-II fluorescence imaging-guided resection and photothermal ablation of lymph nodes," *Adv. Sci.* **8**(9), 2003972 (2021).

28. X. Fan, Q. Xia, Y. Zhang, Y. Li, Z. Feng, J. Zhou, J. Qi, B. Z. Tang, J. Qian, H. Lin, Aggregation-induced emission (AIE) nanoparticles-assisted NIR-II fluorescence imaging-guided diagnosis and surgery for inflammatory bowel disease (IBD)," *Adv. Healthc. Mater.* **10**(24), 2101043 (2021).

29. A. N. Bashkatov, E. A. Genina, V. V. Tuchin, "Optical properties of skin, subcutaneous, and muscle tissues: A review," *J. Innov. Opt. Health Sci.* **04**(01), 9–38 (2011).

30. M. He, D. Li, Z. Zheng, H. Zhang, T. Wu, W. Geng, Z. Hu, Z. Feng, S. Peng, L. Zhu, W. Xi, D. Zhu, B. Z. Tang, J. Qian, Aggregation-induced emission nanoprobe assisted ultra-deep through-skull three-photon mouse brain imaging," *Nano Today* **45**, 101536 (2022).

31. Y. Li, Z. Cai, S. Liu, H. Zhang, S. T. H. Wong, J. W. Y. Lam, R. T. K. Kwok, J. Qian, B. Z. Tang, "Design of AIEgens for near-infrared IIb imaging through structural modulation at molecular and morphological levels," *Nat. Commun.* **11**(1), 1255 (2020).

32. F. Heymann, P. M. Niemietz, J. Peusquens, C. Ergen, M. Kohlhepp, J. C. Mossanen, C. Schneider, M. Vogt, R. H. Tolba, C. Trautwein, C. Martin, F. Tacke, "Long term intravital multi-photon microscopy imaging of immune cells in healthy and diseased liver using CXCR6.Gfp reporter mice," *J. Vis. Exp.* **24**(97), 52607 (2015).

33. M. Zhang, J. Yue, R. Cui, Z. Ma, H. Wan, F. Wang, S. Zhu, Y. Zhou, Y. Kuang, Y. Zhong, D. W. Pang, H. Dai, "Bright quantum dots emitting at ~1,600 nm in the NIR-IIb window for deep tissue fluorescence imaging," *Proc. Natl. Acad. Sci. U.S.A.* **115**(26), 6590–6595 (2018).

34. J. L. Nxumalo, M. Teranaka, W. G. Schenk, "Sensitivity of indocyanine green (ICG) half-life changes relative to circulatory shock state," *J. Surg. Res* **23**(6), 400–404 (1977).

35. A. De Gasperi, E. Mazza, M. Prosperi, "Indocyanine green kinetics to assess liver function: Ready for a clinical dynamic assessment in major liver surgery?" *World J. Hepatol.* **8**(7), 355–367 (2016).

36. R. Marchesini, A. Bertoni, S. Andreola, E. Melloni, A. E. Sichirollo, "Extinction and absorption coefficients and scattering phase functions of human tissues *in vitro*," *Appl. Opt.* **28**(12), 2318–2324 (1989).

37. B. Gysbrechts, L. Wang, N. N. Trong, H. Cabral, Z. Navratilova, F. Battaglia, W. Saeys, C. Bartic, "Light distribution and thermal effects in the rat brain under optogenetic stimulation," *J. Biophoton.* **9**(6), 576–585 (2016).

38. F. Wang, H. Wan, Z. Ma, Y. Zhong, Q. Sun, Y. Tian, L. Qu, H. Du, M. Zhang, L. Li, H. Ma, J. Luo, Y. Liang, W. J. Li, G. Hong, L. Liu, H. Dai, "Light-sheet microscopy in the near-infrared II window," *Nat. Methods* **16**(6), 545–552 (2019).

39. P. E. Marques, M. M. Antunes, B. A. David, R. V. Pereira, M. M. Teixeira, G. B. Menezes, "Imaging liver biology *in vivo* using conventional confocal microscopy," *Nat. Protocol* **10**(2), 258–268 (2015).

40. J. Yu, R. Zhang, Y. Gao, Z. Sheng, M. Gu, Q. Sun, J. Liao, T. Wu, Z. Lin, P. Wu, L. Kang, H. Li, L. Zhang, W. Zheng, "Intravital confocal fluorescence lifetime imaging microscopy in the second near-infrared window," *Opt. Lett.* **45**(12), 3305–3308 (2020).

41. L. Streich, J. C. Boffi, L. Wang, K. Alhalaseh, M. Barbieri, R. Rehm, S. Deivasigamani, C. T. Gross, A. Agarwal, R. Prevedel, "High-resolution structural and functional deep brain imaging using adaptive optics three-photon microscopy," *Nat. Methods* **18**(10), 1253–1258 (2021).

42. Y. Hontani, F. Xia, C. Xu, "Multicolor three-photon fluorescence imaging with single-wavelength excitation deep in mouse brain," *Sci. Adv.* **7**(12), eabf3531 (2021).

43. K. Choe, Y. Hontani, T. Wang, E. Hebert, D. G. Ouzounov, K. Lai, A. Singh, W. Béguelin, A. M. Melnick, C. Xu, "Intravital three-photon microscopy allows visualization over the entire depth of mouse lymph nodes," *Nat. Immunol.* **23**(2), 330–340 (2022).

44. M. A. Yaseen, J. Sutin, W. Wu, B. Fu, H. Uhlirova, A. Devor, D. A. Boas, S. Sakadžić, "Fluorescence lifetime microscopy of NADH distinguishes alterations in cerebral metabolism *in vivo*," *Biomed. Opt. Express* **8**(5), 2368–2385 (2017).